Using Density Functional Theory to Rationally Design Ru(II)-Polypyridyl Complexes for Nitrile Ligand Loss

Undergraduate Research Thesis

Presented in partial fulfillment of the requirements for graduation with honors research distinction in Chemistry in the undergraduate colleges of The Ohio State University

by

Haley Palm

The Ohio State University

May 2017

Project Advisor: Dr. Claudia Turro, Department of Chemistry and Biochemistry

Abstract

Photodynamic therapy (PDT) is an emerging cancer therapy that utilizes photoactive drug molecules, which can be activated with low energy light but are otherwise inactive. Previous studies show that ruthenium(II) complexes with ancillary nitrile ligands are a promising tool in PDT due to their rapid photodissociative properties, which allows for selective delivery of therapeutic agents.[1] If the dissociative nature of this bond can be tuned, these compounds could serve in the development of novel oncological treatments. This study aims to analyze the effects of various bidentate ligands on the bond strength of acetonitrile bound to a ruthenium(II) metal center and to determine which parameters most account for efficient nitrile ligand loss. A series of six ruthenium(II)-polypyridyl complexes, each with a different bipyridyl derivative, were subjected to singlet and triplet state geometry optimizations using B3LYP functional and a combination of the 6-31G* and SDD basis sets. The Mayer bond orders and bond lengths of the nitrile bond and the percent metal character in each derivative were calculated and compared to assess which bidentate ligand results in the greatest destabilization of the acetonitrile bond. It was determined that nitrile ligand loss occurs from the triplet state, and that complexes with more metal-centered character in the excited state will likely undergo more efficient nitrile ligand loss, but further studies are required.

Introduction

Currently, one of the most effective anticancer agents for a wide variety of cancers is cisplatin, *cis*-[$Pt(NH_3)Cl_2$], and its derivatives.[2-7] Upon entering the cell, cisplatin is activated, at which point it exchanges both chloride ligands for two water molecules. In its hydrated form, the molecule can bind to the DNA bases causing irreparable damage, interrupting cell reproduction and triggering cell death. The process by which the chloride and water exchange occurs is

induced thermally, which allows the drug to be targeted at rapidly reproducing cells.[5-7] But this treatment is nonspecific; many healthy cells in the body, such as liver and hair cells, also reproduce quickly. These healthy cells are attacked by the cisplatin, leading to varying undesirable and potentially life-threatening side effects.[6-7] Furthermore, cisplatin only shows specificity for certain types of cancer, such as ovarian or testicular cancer, limiting its versatility. The more aggressive cancers that it does treat effectively, like breast cancer, are known to develop a resistance to the drug, complicating treatment in the event of a recurrence.[2-7]

To avoid the adverse effects related to cisplatin-based treatments, novel oncological methods are being explored. Currently, photodynamic therapy (PDT) is at the forefront of these new FDA-approved techniques. Drug molecules involved in PDT are otherwise nontoxic until activated by excitation with low energy visible light.[8-10] Able to permeate up to 2 cm of skin, low energy visible light (ca. 600-900 nm) is an optimal choice for activation of these drug molecules in most bodily tissue, including cells, membranes, or in proximity of the tumor, allowing for general localization to the cancerous area.

Ru(II)-polypyridyl complexes have been extensively studied for the past several decades for their novel electro- and photochemical properties. Their high extinction coefficients and long-lived excited states give rise to an increased probability of electronic excitation and resulting photochemical transitions, producing unique reaction possibilities.[11] Furthermore, they are well-known to undergo rapid photoinduced nitrile ligand dissociation.[12-15] When irradiated with low energy visible light, the complex is excited from the ^{1}GS (singlet ground state) to a high energy ^{1}MLCT (singlet metal-to-ligand charge transfer) state, quickly undergoing intersystem crossing to the ^{3}MLCT (triplet metal-to-ligand charge transfer) state with unity quantum yield. At this

point, the ^{3}MC (triplet metal centered) state is available for thermal population, allowing for ligand dissociation.[16] The capability of Ru(II) compounds to undergo excited state ligand loss makes them ideal models for improving PDT, as they allow for specific photoactivated delivery of bound therapeutic molecules.

Density Functional Theory (DFT) is a computational quantum mechanical modeling method by which these potential Ru(II) complexes can be theoretically optimized and studied, providing a method to rationally design new and effective Ru(II)-based PDT agents. DFT utilizes the variational principle – a method by which to find functions that optimize quantities dependent on those functions – to sift through all eligible wavefuctions in order to select a subset from which to then systematically minimize the energy functional $E[\Psi]$, optimizing the single point energy of the molecule.[17]

When the initial structure is input into the program, the initial system is perturbed by changing the atom position. Then, the wavefunction at the new atom position is recalculated and the new single point energy of the molecule is determined. If the energy of the perturbed structure is higher than that of the initial structure, the molecule is returned to its original structure and the perturbation cycle begins again, now changing the system in a different manner. If the new energy is lower, however, the perturbed structure is kept and cycled through again. This process continues until a minimum is found, where each new round of perturbation results in increased single point energy of the molecule, indicated by the peaks shown in Figure 1. At this point, the system is considered optimized and the final structure is returned. After a structure is optimized, the second derivative of the output (Figure 1) is then calculated to ensure that the structure has reached an energy minimum and not a saddle point.

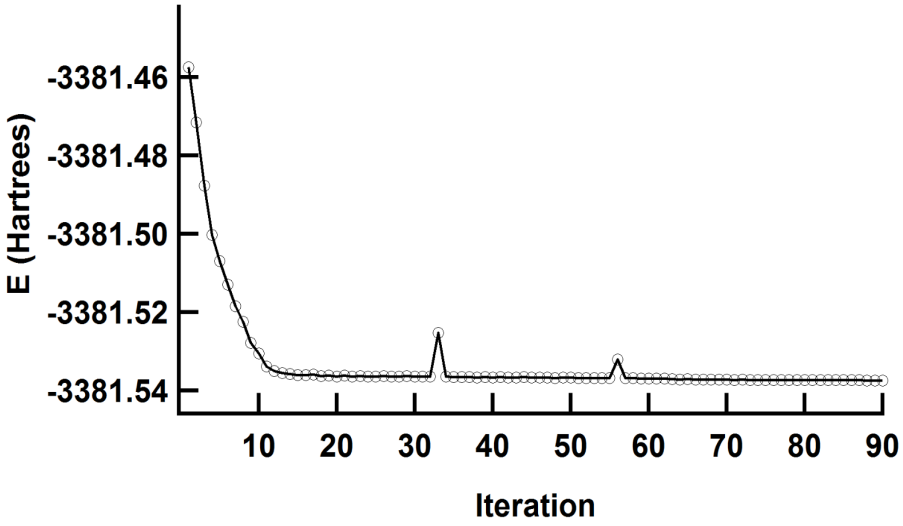

Figure 1: Example output for an optimization calculation.

Coupled with other calculation programs like AOMix, DFT becomes a powerful tool in determining the effect of an infinite number of parameters on the chemistry of a particular molecule. By studying a series of analogue molecules, especially in the context of empirical data and established trends, comparisons can be made to investigate exactly why a molecule exhibits a certain behavior, which in this study is nitrile ligand loss. If it can be determined which factors are responsible for a behavior, then that behavior can be tuned to optimize those properties. This ability of DFT makes it an invaluable device in the design of new molecules for PDT.

The complexes under investigation are $[Ru(tpy)(bpy)(NCCH_3)]^{2+}$ (**Bpy, 1;** tpy = 2,2':6',2''-terpyridine, bpy = 2,2'-bipyridine), $[Ru(tpy)(Mebpy)(NCCH_3)]^{2+}$ (**Mebpy, 2;** mebpy = 6,6'-dimethyl-2,2'-bipyridine), $[Ru(tpy)(OTOpy)(NCCH_3)]^{2+}$ (**OTOpy, 3;** OTOpy = 2-(pyridine-2-yl)-1,3-O-oxathiane), $[Ru(tpy)(OTSpy)(NCCH_3)]^{2+}$ (**OTSpy, 4;** 2-(pyridine-2-yl)-1,3-S-oxathiane), $[Ru(tpy)(Acpy)(NCCH_3)]^{+}$ (**Acpy, 5;** 2-pyridinecarboxylate), $[Ru(tpy)(Thiopy)(NCCH_3)]^{2+}$ (**Thiopy, 6;** Thiopy = 6-(2-thienyl)-pyrindine), and their molecular structures are shown in Figure 2. Complexes were investigated in pairs (**1** and **2**, **3** and **4**, **5** and

6) to better compare the nitrile ligand lability.

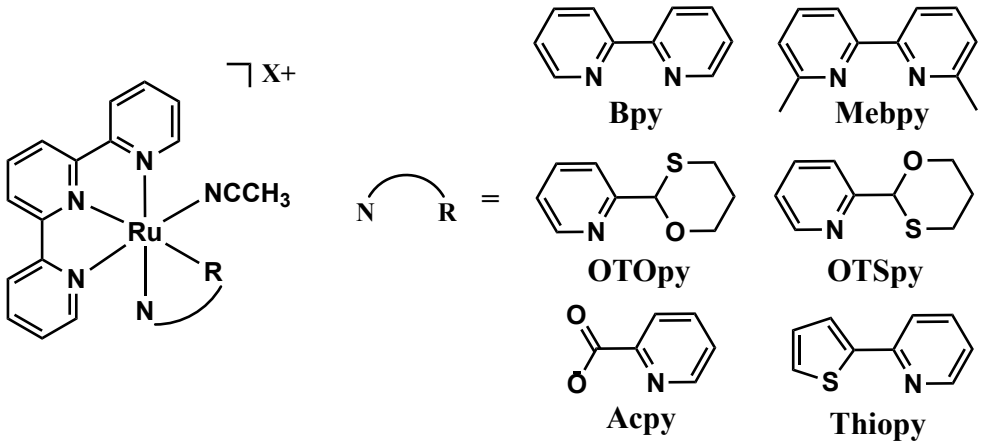

Figure 2: The proposed complexes for study: (1) $[Ru(tpy)(bpy)(NCCH_3)]^{2+}$, (2) $[Ru(tpy)(Mebpy)(NCCH_3)]^{2+}$, (3) $[Ru(tpy)(OTOpy)(NCCH_3)]^{2+}$, (4) $[Ru(tpy)(OTSpy)(NCCH_3)]^{2+}$, (5) $[Ru(tpy)(Acpy)(NCCH_3)]^{+}$, and (6) $[Ru(tpy)(Thiopy)(NCCH_3)]^{2+}$.

Experimental Methods

All molecules were first subjected to loose and tight geometry optimizations. Then, force constant calculations were run to ensure that the optimized structures were not at energy saddle points ($\Delta E = 10^{-7} – 10^{-10}$). Frequency and time-dependent DFT analyses were also conducted to ensure the absence of imaginary frequencies or wavelengths. Finally, electron density plots were generated and Mayer bond orders, bond lengths, and percent metal character for each structure were calculated.

DFT optimizations were run using B3LYP functional and 6-31g* for all non-metal atoms and the Stuttgart-Dresden energy-consistent pseudo-potential for the ruthenium atoms for the singlet and triplet states using Gaussian 09. Triplet state calculations were treated with UB3LYP, which analyzes the electron spins individually by dividing the orbitals, instead of forcing the electrons to be spin-paired as in B3LYP. AOMix was used to calculate Mayer bond orders, bond lengths, and percent fragment characters.

Results and Discussion

The data suggests that ligand loss occurs from the triplet manifold of states through a process controlled by kinetics, as diagrammed in Figure 3.

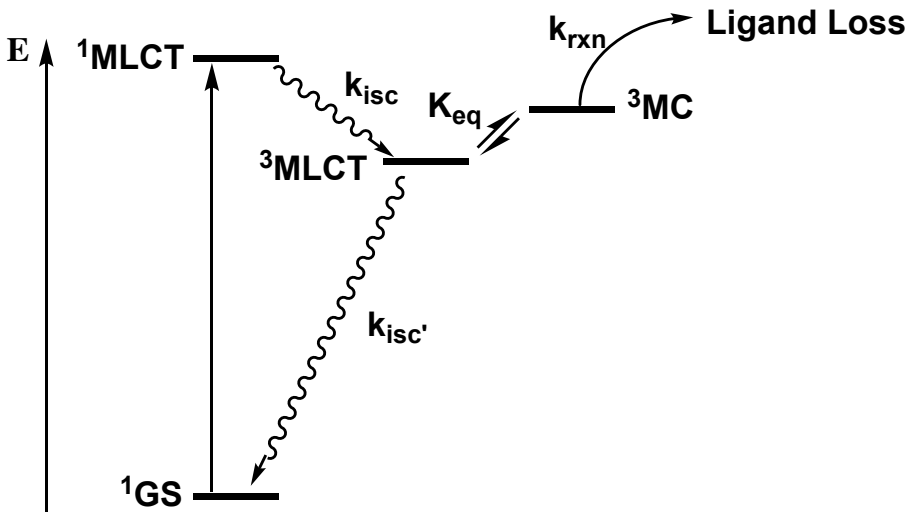

Figure 3: Jablonski Diagram of Ru(II)-polypyridyl excited state manifold where more ^{3}MC character leads to more efficient ligand loss.

The mechanism by which the nitrile ligand loss occurs (Figure 3) begins typically, with the initial ^{1}MLCT excitation from the ^{1}GS and rapid intersystem crossing to ^{3}MLCT, which is expected to populate within 40 femtoseconds with unit efficiency.[18] From this state, the ^{3}MC state is thermally accessible and elimination of the nitrile ligand becomes possible. It is expected that dissociation will occur from the ^{3}MC state due to increased metal character in the excited state of the complexes, discussed later.

Mayer bond order, which is an extension of the Wiberg bond order and Mulliken population analysis,[19] describes the covalency of the bond on a scale of zero to one with zero being most ionic and one being most covalent, and bond lengths were investigated initially, under the postulation that complexes containing longer and more ionic ruthenium-nitrile bonds would result in more efficient ligand loss. Under this assumption, the data presented in Table 1 would

then indicate that $[Ru(tpy)(bpy)(NCCH_3)]^{2+}$, $[Ru(tpy)(OTOpy)(NCCH_3)]^{2+}$, and $[Ru(tpy)(Acpy)(NCCH_3)]^{+}$ would all undergo more rapid ligand elimination because they have longer and more ionic bonds in the excited triplet state, as compared to the singlet ground state. However, it has been previously shown[16] that $Ru(tpy)(Mebpy)(NCCH_3)]^{2+}$ has a much lower ^{3}MC state than $[Ru(tpy)(bpy)(NCCH_3)]^{2+}$, and therefore undergoes more facile ligand loss, which is contrary to the bolded data, so this process is likely not controlled by bond distance or bond covalency.

	Bpy		**Mebpy**		**OTOpy**		**OTSpy**		**Acpy**		**Thiopy**	
State	^{1}GS	^{3}MC	^{1}GS	^{3}MC	^{1}GS	^{3}MC	^{1}GS	^{3}MC	^{1}GS	^{3}MC	^{1}GS	^{3}MC
Mayer Bond Order	0.489	**0.447**	0.493	**0.450**	0.508	0.498	0.521	0.510	0.520	0.480	0.519	0.503
Bond Distance	2.048	**2.060**	2.045	**2.058**	2.040	2.044	2.034	2.039	2.039	2.058	2.038	2.056

Table 1: Mayer bond orders and bond distances for the ruthenium-nitrile bond of each complex in both the singlet and triplet states.

The electron density maps (Figures 4-9) and the percent fragment character data (Table 2) also suggest that the nitrile ligand loss occurs as a results of greater access to a low-lying ^{3}MC state, resulting in favorable rates of ligand loss.

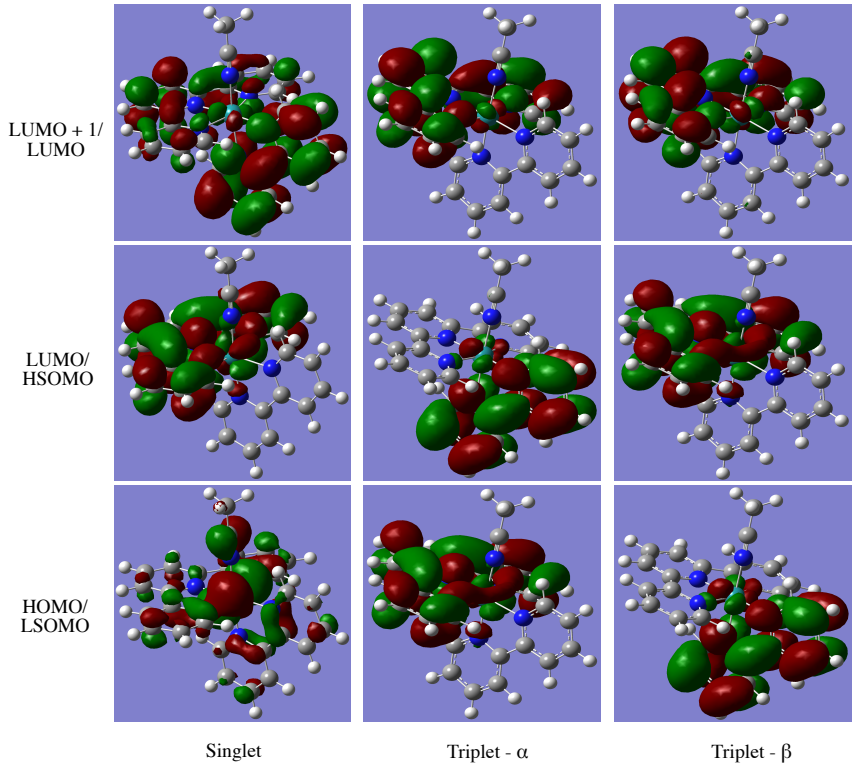

Figure 4: Electron density maps of selected MO calculations of $[Ru(tpy)(bpy)(NCCH_3)]^{2+}$ (isoval=0.04).

Figure 4 above shows the electron density plot for $[Ru(tpy)(bpy)(NCCH_3)]^{2+}$. The superimposed red and green surfaces indicate areas of electron density, with the different colors representing the two different electronic phases. The process diagrammed in Figure 3 can be followed through these maps. Beginning with the initial ^{1}MLCT excitation from the ^{1}GS in the singlet diagrams, the electron density shifts from the central ruthenium atom (HOMO) to the terpyridine ligand (LUMO), corresponding to a shift from a nonbonding dπ interaction to an antibonding π* interaction. The intersystem crossing to the ^{3}MLCT state is then seen in the Triplet – α (HSOMO) diagram, where the density has transferred to the bipyridine ligand, which is also an antibonding π* interaction. The other compounds (Figures 5-9) follow similarly, though not all complexes show electron density movement during the intersystem crossing to the ^{3}MLCT state, as the electron density remains on the terpyridine ligand during this electronic event for the OTOpy and OTSpy compounds. However, the more significant differences are in the amount of

density remaining on the ruthenium atom in the excited triplet manifold for each complex. For each complex pair, $[Ru(tpy)(Mebpy)(NCCH_3)]^{2+}$, $[Ru(tpy)(OTOpy)(NCCH_3)]^{2+}$, and $[Ru(tpy)(Thiopy)(NCCH_3)]^{2+}$ all show more ruthenium character in the excited triplet state, which is supported by the data presented in Table 2.

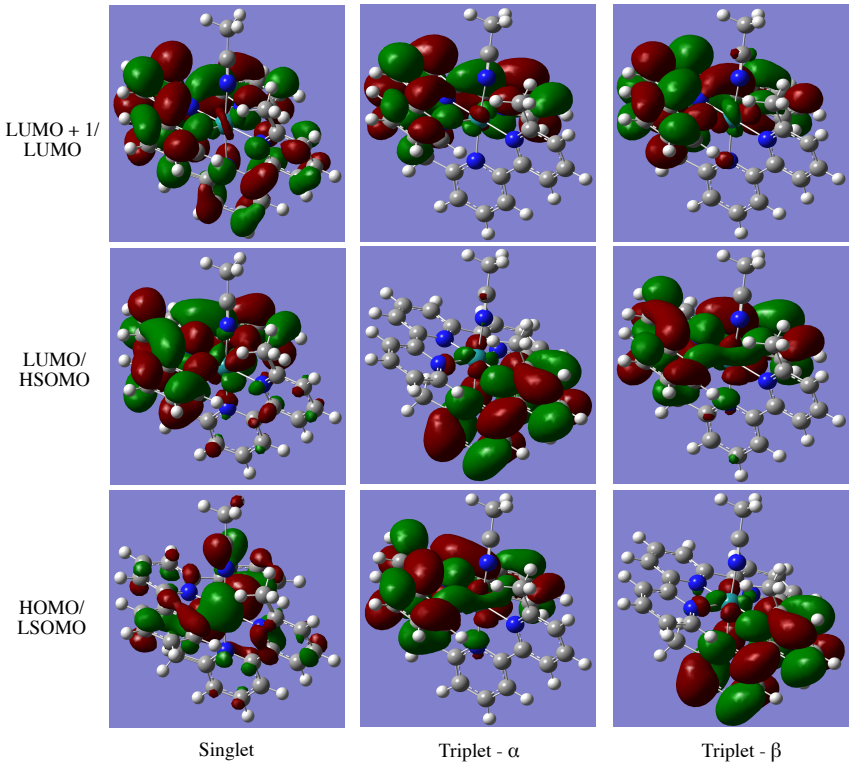

Figure 5: Electron density maps of selected MO calculations of $[Ru(tpy)(Mebpy)(NCCH_3)]^{2+}$ (isoval=0.04).

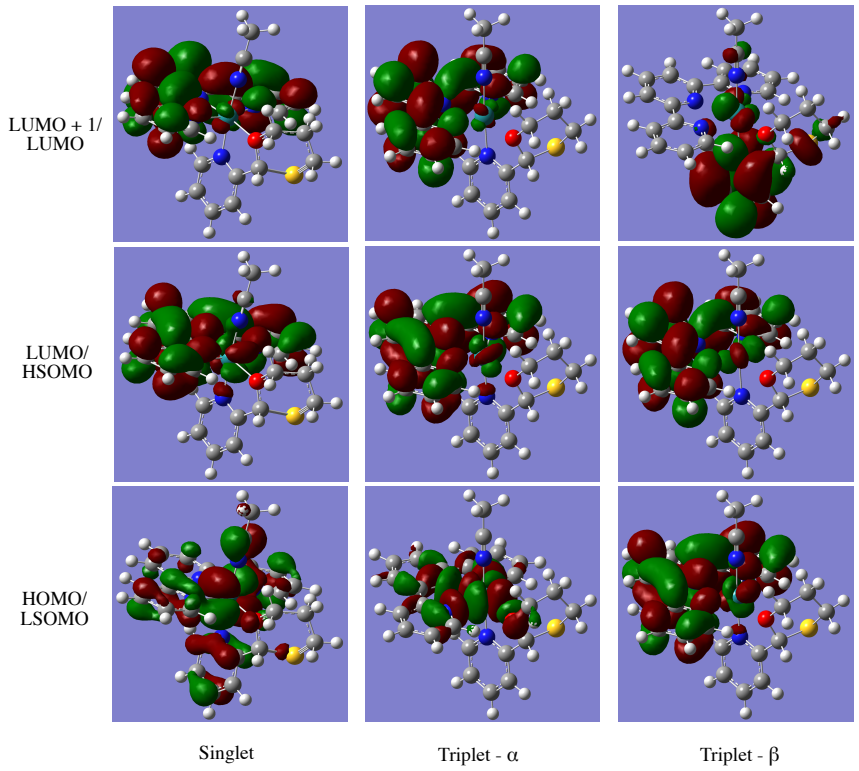

Figure 6: Electron density maps of selected MO calculations of $[Ru(tpy)(OTOpy)(NCCH_3)]^{2+}$ (isoval=0.04).

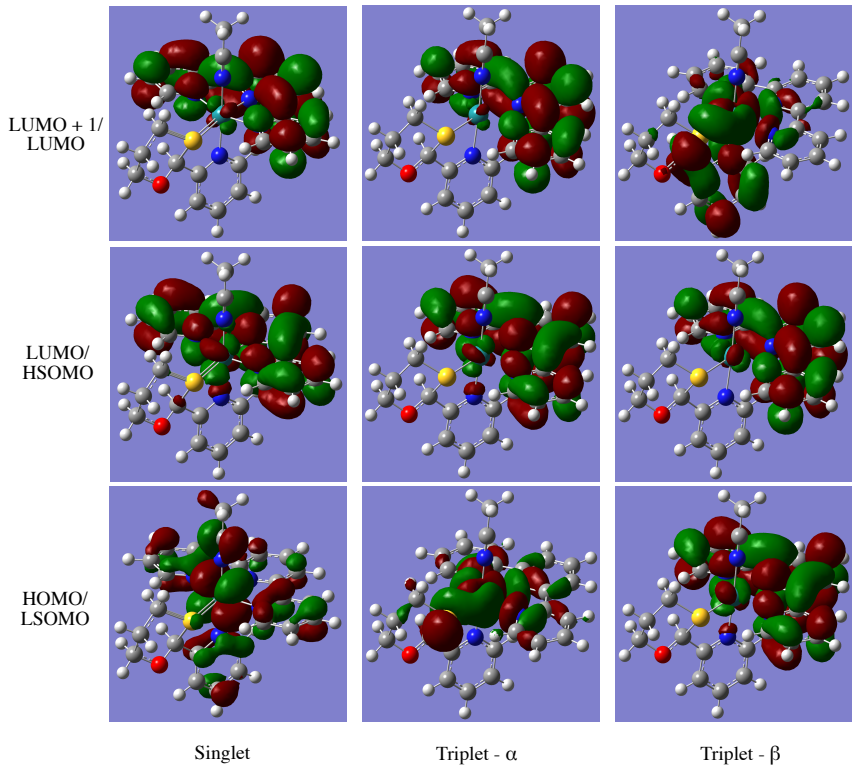

Figure 7: Electron density maps of selected MO calculations of $[Ru(tpy)(OTSpy)(NCCH_3)]^{2+}$ (isoval=0.04).

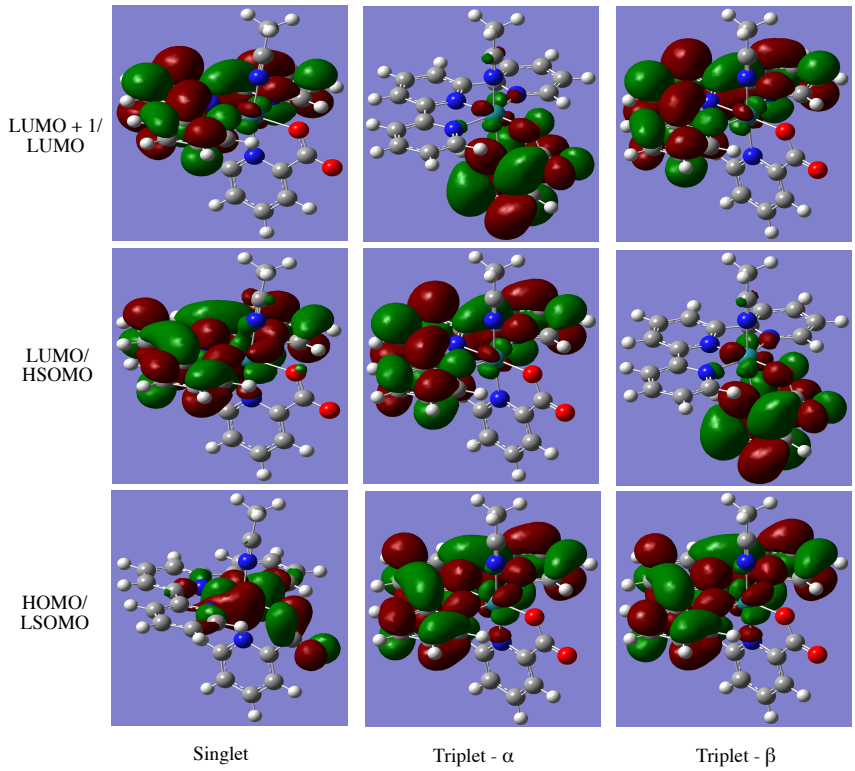

Figure 8: Electron density maps of selected MO calculations of $[Ru(tpy)(Acpy)(NCCH_3)]^+$ (isoval=0.04).

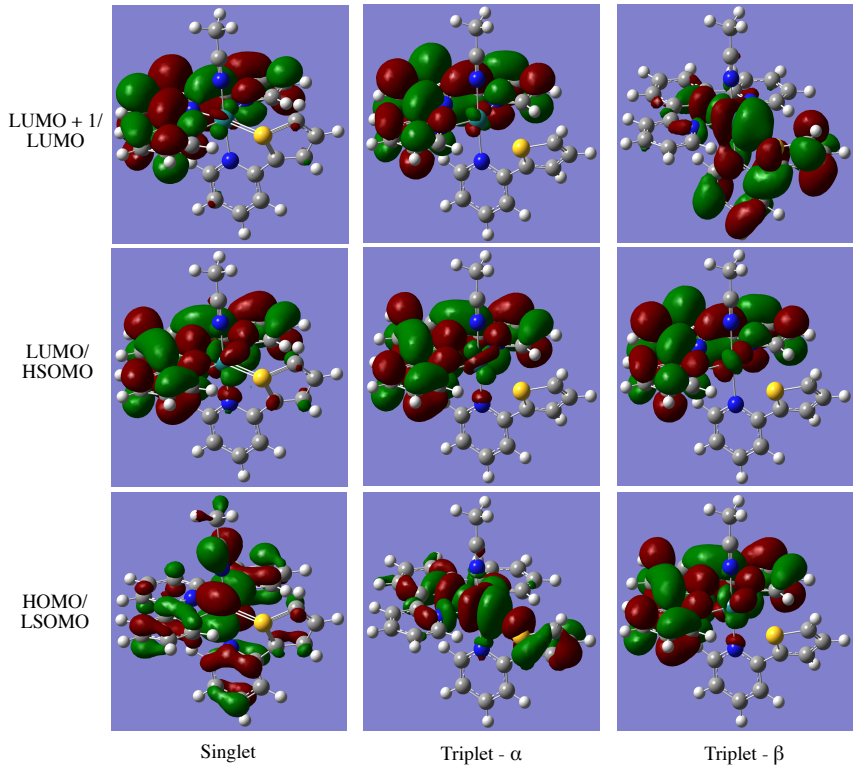

Figure 9: Electron density maps of selected MO calculations of $[Ru(tpy)(Thiopy)(NCCH_3)]^{2+}$ (isoval=0.04).

Because these Ru(II) complexes are low-spin d^6 pseudo-octahedral systems, inducing a photoexcited state requires promoting an electron from the completely filled t_{2g}-like orbitals to the empty e_g t_{2g}-like orbitals. Promoting this electron means shifting electron density from a more stable nonbonding orbital to a less stable antibonding orbital. Moreover, the t_{2g}-like orbitals lie between the xyz axes, whereas the two e_g-like orbitals lie directly along the axes, so exciting an electron puts more electron density directly in conflict with the density on the central ruthenium atom, increasing the electron-electron repulsions. Taken together, these effects significantly destabilize the ruthenium-nitrile bond, reducing the activation energy for ligand loss and increasing the efficiency.

These electronic effects suggest that complexes with more ruthenium character in the excited triplet state should then undergo more rapid nitrile ligand loss. This assertion is supported by the bolded data in Table 2, which shows the percent metal character in each state for all derivatives.

		Bpy		Mebpy	
		^{1}GS	^{3}MC	^{1}GS	^{3}MC
%Ru Character	HOMO/LSOMO	76.10	**8.62**	76.25	**10.77**
	LUMO/HSOMO	6.11	38.15	5.54	38.09
	LUMO+1/LUMO	2.38	2.41	1.49	2.08
%Tpy Character	HOMO/LSOMO	13.05	89.84	14.20	86.94
	LUMO/HSOMO	93.01	8.51	89.51	9.50
	LUMO+1/LUMO	26.54	49.93	77.76	50.47
		OTOpy		**OTSpy**	
		^{1}GS	^{3}MC	^{1}GS	^{3}MC
%Ru Character	HOMO/LSOMO	72.22	**69.38**	73.01	**67.68**
	LUMO/HSOMO	6.55	43.24	4.86	43.31
	LUMO+1/LUMO	1.20	2.47	1.23	2.22
%Tpy Character	HOMO/LSOMO	14.26	20.42	15.17	18.85
	LUMO/HSOMO	92.39	53.25	92.89	52.48
	LUMO+1/LUMO	98.38	97.13	98.40	96.98
		Acpy		**Thiopy**	
		^{1}GS	^{3}MC	^{1}GS	^{3}MC
%Ru Character	HOMO/LSOMO	75.99	**31.27**	70.94	**65.36**
	LUMO/HSOMO	7.99	39.21	5.00	45.20
	LUMO+1/LUMO	1.33	3.17	1.19	2.79
%Tpy Character	HOMO/LSOMO	8.38	62.60	15.14	18.44
	LUMO/HSOMO	90.54	54.24	91.42	52.90
	LUMO+1/LUMO	98.09	47.56	96.38	96.42

Table 2: Percent ruthenium and terpyridine character for selected MO calculations for each complex.

The bolded data comparing $Ru(tpy)(bpy)(NCCH_3)]^{2+}$ and $[Ru(tpy)(Mebpy)(NCCH_3)]^{2+}$ clearly indicates that the excited triplet manifold for $[Ru(tpy)(Mebpy)(NCCH_3)]^{2+}$ contains greater Ru(^{3}MC) character than $[Ru(tpy)(bpy)(NCCH_3)]^{2+}$, meaning that under this assertion, the Mebpy complex should undergo more rapid nitrile ligand loss. This is supported by experimental data in which Turro and coworkers have previously shown through quantum yield studies that the ^{3}MC state is more accessible for sterically bulky Ru(II)-polypyridyl complexes, with the quantum yield of pyridine loss – an analogue for the nitrile ligand – increasing from <0.0001 to 0.16 at 500 nm when comparing Bpy and Mebpy compounds respectively.[16] Because Mebpy is a larger, more restricted ligand, the e_g-like σ^* orbitals decrease in energy due to reduced overlap,

making them more energetically accessible. Given this trend, the OTOpy and Thiopy complexes should yield more rapid ligand loss than the OTSpy and Acpy analogues.

To confirm these computational studies, further practical experiments, such as the determination of excited state lifetimes and the quantum yield of ligand loss, are currently underway to assess the rate of ligand elimination for these compounds. Additional parameters such as density-gradient densities, Mulliken spin densities, and π-backbonding are also being investigated to establish their impact on nitrile ligand loss efficiency. It is expected that complexes with greater degrees of π-backbonding and more disparity in the densities will achieve more efficient nitrile ligand loss.

Conclusions

$[Ru(tpy)(bpy)(NCCH_3)]^{2+}$, $[Ru(tpy)(Mebpy)(NCCH_3)]^{2+}$, $[Ru(tpy)(OTOpy)(NCCH_3)]^{2+}$, $[Ru(tpy)(OTSpy)(NCCH_3)]^{2+}$, $[Ru(tpy)(Acpy)(NCCH_3)]^{+}$, and $[Ru(tpy)(Thiopy)(NCCH_3)]^{2+}$ were investigated to determine which parameters most account for efficient nitrile ligand loss. It was determined that increased ^{3}MC character, which is responsible for efficient nitrile ligand loss, was seen in $[Ru(tpy)(Mebpy)(NCCH_3)]^{2+}$, $[Ru(tpy)(OTOpy)(NCCH_3)]^{2+}$, and $[Ru(tpy)(Thiopy)(NCCH_3)]^{2+}$. Further studies are underway to affirm these assertions and explore other parameters, leading to a cohesive process for the rational design of PDT agents.

Acknowledgements

I would like to thank my thesis advisor, Dr. Claudia Turro, for allowing me to work and learn in her lab. I would also like to thank my project mentor, Tyler Whittemore, for his invaluable support and guidance on this project. Additionally, I am forever grateful to Dr. Terry Gustafson, who first encouraged my pursuit of research.

References

[1] Knoll, J. D.; Turro, C. *Coord. Chem. Rev.* **2015**, 282-283, 110 – 126.

[2] Oliver, T.; Mead, T. *Curr. Opin. Oncol*. 5 **(1993)** 559 – 567.

[3] Statopoulous, G.; Rigatos, S.; Melamos, N. A. *Oncol. Rep*. 6 **(1999)** 797 – 800.

[4] Bruhn, S.L.; Toney, J.H.; Lippard, S.J. *Prog. Inorg. Chem*. 38 **(1990)** 477 – 516.

[5] Kellard, L. R.; Farrell, N. P. *Platinum-based Drugs in Cancer Therapy*, Humana Press, N. J., 2000.

[6] Masters, J. R.; Köberle, B. *Nat. Rev. Cancer* 3 **(2003)** 517 – 525.

[7] Jung, Y.; Lippard, S. J. *J. Chem. Rev*. 107 **(2007)** 1387 – 1407.

[8] Juzeniene, A.; Peng, Q.; Moan, J. *Photochem. Photobiol. Sci*. 6 **(2007)** 1234 – 1245. 25

[9] DeRosa, M. C.; Crutchley, R. J. *Coord. Chem. Rev.* 233 – 234 **(2002)** 351 – 371. 26

[10] Detty, M. R.; Gibson, S. L.; Wagner, S. J. *J. Med. Chem.* 47 **(2004)** 3897 – 3915. 27

[11] Juris, A.; Balzani, V.; Barigelletti, F.; Campagna, S.; Belser, P.; von Zelewsky, A. *Coord. Chem. Rev.* 84 **1988**, 85–277.

[12] Ford, P. C. *Coord. Chem. Rev*. 44 **(1982)** 61 – 82. 30

[13] Tfouni, E. *Coord. Chem. Rev*. 196 **(2000)** 231 – 305. 31

[14] Van Houten, J.; Watts, R. J. *Inorg. Chem*. 17 **(1978)** 588 – 593. 32

[15] Durante, V.A.; Ford, P. C. *Inorg. Chem*. **1978** 18, 3381 – 3385. 33

[16] Knoll, J. D.; Albani, B. A.; Turro, C. *Acc. Chem. Res.* **2015**, 48(8), 2280 – 2287.

[17] Koch, W.; Holthausen, M. C. *A Chemist's Guide to Density Functional Theory*; Wiley-VCH: Weinheim, 2010.

[18] Bhasikuttan, A. C.; Suzuki, M.; Nakashima, S.; Okada, T. *J. Am. Chem. Soc.* **2002** *124* (28), 8398-8405

[19] Bridgeman, A. J.; Cavigliasso, G.; Ireland, L. R.; Rothery, J. *Dalton Trans.* **2001**, 14, 2095–2108.